Research Square

Preprints are preliminary reports that have not undergone peer review.
They should not be considered conclusive, used to inform clinical practice,
or referenced by the media as validated information.

Monitoring-based assessment of spatial and seasonal air-quality associations with low-emission zones in South Korea

Minju Lee
Ewha Womans University
Mijeong Kim
m.kim@ewha.ac.kr

Ewha Womans University

Research Article

Keywords: Environmental surveillance, Nitrogen dioxide, Ozone, Spatial Durbin model, Pre-adoption trends, Measurement uncertainty

Posted Date: November 4th, 2026

DOI: https://doi.org/10.21203/rs.3.rs-11330159/v1

License: This work is licensed under a Creative Commons Attribution 4.0 International License.
Read Full License

Additional Declarations: No competing interests reported.

Monitoring-based assessment of spatial and seasonal air-quality associations with low-emission zones in South Korea

Minju Lee[1] and Mijeong Kim[1*]

[1]Department of Statistics, Ewha Womans University, Seoul, 03760, South Korea.

*Corresponding author(s). E-mail(s): m.kim@ewha.ac.kr;
Contributing authors: mjstg23@ewhain.net;

Abstract

Regional assessments of vehicle restrictions rely on both the construction of concentration fields from monitoring stations and the comparability of policy and comparison areas. We integrate these two dimensions of assessment using monthly concentrations of five pollutants in 247 South Korean districts during 2012–2024. Quality-screened station observations are interpolated and area-weighted to districts, with precipitation reconciled against published monthly totals. Station-holdout validation and a common-grid nearest-station alternative assess measurement sensitivity. Spatial Durbin models assess pooled and seasonal associations while accounting for spatial dependence and district and year-month fixed effects. Baseline models associate permanent low-emission-zone rollout with lower nitrogen dioxide concentrations; trend-adjusted models show that regional trajectories are central to interpreting this finding. Associations also differ across pollutants and seasons, with some patterns depending on interpolation choice. Pre-adoption differences support interpreting these estimates as conditional associations rather than causal effects. This study provides an integrated, reproducible framework for evaluating low-emission zones, characterizing pollutant-specific spatial and seasonal associations while distinguishing sensitivity to measurement choices from sensitivity to regional-trend assumptions.

Keywords: Environmental surveillance, Nitrogen dioxide, Ozone, Spatial Durbin model, Pre-adoption trends, Measurement uncertainty

Introduction

Routine air-quality monitoring provides the observations needed to assess how environmental conditions change alongside urban vehicle restrictions. Low-emission zones (LEZs), which restrict access by qualifying high-emitting vehicles, are one such intervention. Their environmental relevance extends beyond traffic management to the distribution of ambient pollution in populated regions (Nieuwenhuijsen, 2016). Interpreting observed concentration changes requires attention to meteorology, atmospheric chemistry, regional transport, other sources, and concurrent policies alongside the restriction itself. The heterogeneous findings in the LEZ literature consequently motivate pollutant-specific assessment that accommodates these influences (Holman, Harrison, & Querol, 2015).

Three complementary dimensions motivate an integrated use of monitoring data. First, seasonal resolution captures differences in chemical and dispersion conditions that annual averages combine. Korean observations identify a May–June ozone maximum and geographically varying chemical regimes (Oak et al., 2025); separate seasonal estimates can reveal patterns concealed by a pooled association. Second, vehicle movements and atmospheric transport extend across administrative borders. Accounting for spatially correlated outcomes and neighboring restrictions therefore complements conventional difference-in-differences (DID) comparisons (Delgado & Florax, 2015). Third, concentrations observed at stations must be translated to the geographic units used for policy assessment. Spatial interpolation and district aggregation form a measurement layer that can be evaluated through prediction validation alongside the statistical model linking concentrations to designation.

South Korea's phased permanent-LEZ expansion provides a setting in which to investigate these issues using a common monthly panel. Designation expanded from Seoul to parts of Incheon and Gyeonggi and subsequently to further Gyeonggi cities. Related Korean studies examine Seoul's geographically narrower ultra-low-emission zone and the broader Clean Air Act (Im, Jang, Kim, & Hong, 2026; Park & Lim, 2025). Those interventions differ from the permanent diesel-vehicle restriction studied here. The question addressed in this study is how station-derived pollution summaries covary with the latter designation across pollutants, seasons, and geographic neighbors, and whether those descriptions persist under alternative regional-trend assumptions.

Geographically targeted rollout makes pre-adoption trajectories important: metropolitan jurisdictions may already have followed different pollution paths. We use Callaway–Sant'Anna group-time comparisons to assess pre-adoption comparability (Callaway & Sant'Anna, 2021) and spatial Durbin models (SDMs) to describe

own-unit and cross-unit associations (Elhorst, 2014; LeSage & Pace, 2009). Together, these analyses link spatial patterns to the assumptions needed for policy attribution.

This study contributes to assessment of the Korean rollout in three respects. First, it connects quality-screened monitoring records to district concentration fields through documented coverage rules, precipitation reconciliation, and held-out prediction validation. Second, using five pollutants in 247 districts during 2012–2024, it compares interpolation methods on common spatial support and baseline and cohort-trend models within each construction, separating measurement sensitivity from regional-trend sensitivity. Third, spatial decomposition and covariance-aware seasonal tests characterize cross-district and within-year differences that pooled, non-spatial summaries can conceal. This pollutant-specific approach accommodates nonlinear ozone chemistry and mixed particulate sources, which can produce positive, negligible, or uncertain associations (Bessagnet et al., 2024; Seinfeld & Pandis, 2016).

Materials and methods

Study setting and permanent-LEZ rollout

The policy of interest is the permanent restriction on qualifying old diesel vehicles, not seasonal-management restrictions, emergency measures, or Seoul's green-transport-zone scheme. The 2016 intergovernmental announcement specified Seoul-wide expansion in 2017, Incheon and 17 Gyeonggi cities in 2018, and further Gyeonggi cities by 2020 (Ministry of Environment, 2016). The national vehicle-emissions information system describes integrated second-stage operation from 1 July 2018 (MECAR, n.d.). Designation indicates geographic coverage of a restriction subject to vehicle eligibility and exemptions, rather than a prohibition applying immediately to every old diesel vehicle.

We assign the three phases to January 2017, July 2018, and January 2020. A contemporaneous government publication dates Seoul-wide expansion to January 2017, extending geographically narrower pre-existing restrictions (Ministry of Culture, Sports and Tourism, 2017). July 2018 follows the integrated second-stage operation (MECAR, n.d.). The sources establish third-phase expansion by 2020 but not a common first-enforcement month for all 11 cities; January 2020 is therefore a coding assumption. Designation measures geographic rollout, not district-level enforcement intensity or compliance. Timing sensitivity moves the second phase to January 2018, or the third to July or December 2020, in baseline and cohort-trend models. Supplementary Section S8 records the source-to-code mapping and scenarios.

The first cohort comprises Seoul's 25 gu. The second adds nine Incheon units, excluding Ongjin-gun, and 26 analysis units corresponding to the first 17 Gyeonggi cities. The third adds 13 units corresponding to 11 further Gyeonggi cities. Thus, 73 districts are ever designated and 174 are not designated under this permanent-LEZ definition. The latter may nevertheless be exposed to neighboring restrictions and other air-quality policies. Figure 1 distinguishes rollout cohorts; Gyeonggi denotes the province, excluding the separate Seoul and Incheon jurisdictions, not all locations adopting in a single year.

Study panel

The primary balanced panel comprises 247 si-gun-gu units observed from January 2012 through December 2024: 156 months. Si-gun-gu are municipal-level cities, counties, and urban districts. Ongjin-gun and Ulleung-gun, two island counties, are excluded from the 249-unit panel to maintain the common geographic sample. The same sample restriction applies across specifications. District identifiers are harmonized with the geographic file, including province renamings and Gunwi-gun's province affiliation.

The panel contains one observation per district-month and no missing analysis-variable values. The 2013–2024 sensitivity analysis uses the same districts and covariates over the shorter observation window.

Outcomes and covariate adjustment

The outcomes are monthly district-level NO_2, CO, SO_2, O_3, and PM_{10} concentrations constructed from AirKorea's final-confirmed hourly downloads (AirKorea, n.d.). Station locations and network information were retrieved separately from the AirKorea station-information API (Korea Environment Corporation, n.d.). Only the urban ambient series enters the models; roadside series are processed separately. Gases are expressed in parts per billion (ppb) and PM_{10} in $\mu g/m^3$; $PM_{2.5}$ is unavailable. Table 1 summarizes the outcomes and provides pre-adoption reference concentrations for the 73 ever-designated districts, using observations before each district's assigned start month.

Meteorological observations were retrieved through the Korea Meteorological Administration's daily Automated Synoptic Observing System (ASOS) API (Korea Meteorological Administration, n.d.-a) and matched to station coordinates valid on each observation date. Monthly station means of temperature, wind speed, relative humidity, and daily sunshine duration require valid observations on at least 75% of

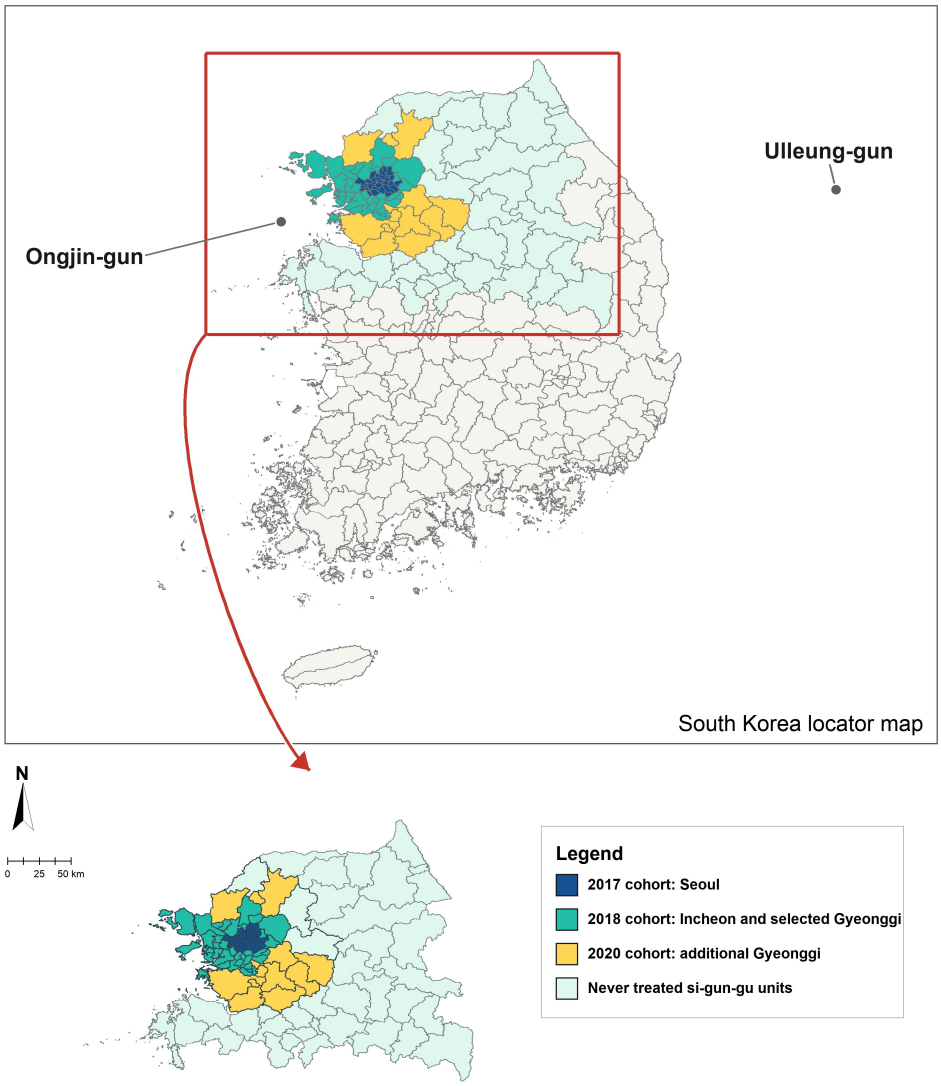


Fig. 1 Study geography and permanent-LEZ rollout cohorts. The monthly assignments are January 2017, July 2018, and January 2020. The inset locates the enlarged map and marks the excluded island counties, Ongjin-gun and Ulleung-gun. Geographic cohort membership is distinct from verified enforcement intensity.

Table 1 Monthly pollutant concentrations in the analysis panel, 2012–2024

Outcome	Mean	SD	Minimum	Maximum	Pre-LEZ mean
NO_2	19.520	7.947	3.799	49.297	29.509
CO	462.525	117.561	173.863	1159.354	550.426
SO_2	3.905	1.464	1.202	15.490	5.200
O_3	28.826	9.535	8.088	60.576	23.928
PM_{10}	40.543	13.462	12.093	96.472	48.752

Notes: All-sample summaries use 38,532 district-months; pre-LEZ means use 5,478 observations before own designation and are not counterfactual values. Gases: ppb; PM_{10}: $\mu g/m^3$. SD: standard deviation.

calendar days. Daily sunshine values outside 0–24 h and station months spanning multiple coordinate records are excluded.

Precipitation is the published station monthly total divided by calendar days (mm/day). Eligible station months require full daily-record coverage, a single coordinate record, and agreement between the numeric daily sum and the published total within 0.051 mm (Korea Meteorological Administration, n.d.-b); unexplained daily blanks are not individually replaced by zero. Before interpolation, low-wind equivalent days are calculated at each station as the proportion of valid daily observations with mean wind speed at or below 2 m/s multiplied by calendar days, requiring at least 75% valid-day coverage. This estimates monthly low-wind days rather than a complete atmospheric-stagnation index and assumes that observed wind days represent the month.

Annual transport and urban variables are obtained from national statistics (Korea Land and Geospatial Informatix Corporation, n.d.; Korea Transportation Safety Authority, n.d.; Ministry of Land, Infrastructure and Transport, n.d.) and repeated across the 12 months of each district-year. Where annual transport and land-use statistics were available only for a parent city, the same city-level value was assigned to its constituent analysis districts. This assignment applies to 30 districts; these covariates therefore do not represent independently observed district-level values. Sejong's 2012 daily vehicle distance is imputed using its 2013–2024 annual mean; the 2013-start and transport-omission models assess related sensitivity. Population density was calculated as annual resident-registration population divided by the fixed district polygon area in square kilometers. The denominator was calculated using spherical geometry. For Seowon-gu, the 2012 and 2013 population totals were reconstructed by summing the constituent eup, myeon, and dong populations. Table 2 lists the 12 controls, each of which also enters as a spatial lag. Continuous controls are standardized within the estimation sample; outcomes and designation remain unscaled.

Table 2 Covariates included in the primary spatial model

Covariate	Analysis variable	Resolution
Mean daily temperature (°C)	`avg_temp`	Monthly
Mean daily sunshine (h/day)	`sun_time`	Monthly
Low-wind equivalent days	`stagnant_days`	Monthly
Mean wind speed (m/s)	`avg_wind`	Monthly
Mean relative humidity (%)	`avg_humid`	Monthly
Mean daily precipitation (mm/day)	`avg_rain`	Monthly
Average daily distance per vehicle	`daily_km`	Annual
Registered cars per capita	`cars_per_capita`	Annual
Population density	`pop_density`	Annual
Industrial area per capita (m^2/person)	`industrial_area`	Annual
Commercial area per capita (m^2/person)	`commercial_area`	Annual
Green area per capita (m^2/person)	`green_area_per_capita`	Annual

Notes: Annual values repeat within district-year. All listed variables and their spatial lags enter Equation (2). Weather labels describe station-level summaries before spatial interpolation; district low-wind-day values can be fractional.

Vehicle distance and car ownership may themselves respond to designation. Conditioning on them can remove part of a policy-related pathway, so we also estimate models excluding both variables and their spatial lags. They are not measures of enforcement. Grade-specific diesel fleets, restricted-vehicle counts, scrappage, and compliance records are unavailable.

Spatial interpolation and validation

Air-pollution station months require valid nonnegative observations for at least 75% of calendar hours; station–month–pollutant groups with duplicate timestamps are excluded. Station metadata are linked by exact code and name matches. Source network labels take precedence, with current-list labels used only when source labels are absent. Current metadata do not establish complete historical station locations or network memberships. Hour-24 observations retain their source reporting month, while official time-interval attribution remains unresolved.

Inverse-distance weighting (IDW) uses power 2 and all eligible stations in each month, with distances calculated in EPSG:5179 meters. Predictions at approximately 2.8-km grid-cell centers are weighted by each cell's intersection area with a district. The fixed 2019 geography contains 14,676 land-intersecting cells and 19,560 district–cell intersections. This procedure approximates a geographic area mean, distinct from a centroid prediction or population-weighted exposure. Interpolation is separate from the geographic weight matrix used in the SDM.

We compare IDW with nearest-station prediction by withholding each station in turn within month. A further precipitation check excludes all stations in the target station's 100-km square grid block; it is not a 100-km distance buffer. For regression sensitivity, a nearest-station field is evaluated at the same cell centers and averaged with the same intersection weights, holding eligible observations, dates, boundaries, and annual covariates fixed. Both pollution outcomes and meteorological covariates are calculated using each method, so this comparison assesses a joint change in environmental measurement, not a pollutant-only change. Point prediction validation does not directly observe the true district mean.

Pre-adoption comparability

Let G_i be district i's assigned first-designation month and define $\text{LEZ}_{it} = \mathbf{1}\{G_i > 0,\ t \geq G_i\}$, with $G_i = 0$ for non-designated districts. Causal DID interpretation requires comparable untreated trajectories, conditional on the identifying assumptions. Before interpreting post-adoption comparisons, we examine whether pre-adoption group-time contrasts are compatible with zero. Callaway–Sant'Anna estimates use not-yet-treated and never-treated comparisons and a universal reference month $G_i - 1$ (Callaway & Sant'Anna, 2021). Outcome-regression adjustment is the primary diagnostic; doubly robust adjustment uses the same sample and controls as a sensitivity analysis. For each two-period DID comparison, covariate adjustment uses values measured in the earlier of the two months. In contrast, the SDM adjusts for covariates measured in the same month as the pollution outcome.

The joint Wald test contains 231 pre-period restrictions for the 2012 start and 195 for the 2013 start, relative to 247 district clusters. We supplement it with a maximum-$|t|$ statistic using the same contrasts and 1,999 district-level Rademacher multiplier draws, avoiding inversion of the high-dimensional contrast covariance. These diagnostics and simultaneous event-study bands use independent district multipliers and do not adjust for cross-district dependence or policy interference. Supplementary Section S1 supplies the formulas.

Spatial specification and estimand

For one pollutant at a time, the non-spatial benchmark is

$$Y_{it} = \alpha_i + \delta_t + \beta \text{LEZ}_{it} + \mathbf{x}'_{it}\gamma + \varepsilon_{it}. \tag{1}$$

Here α_i is a district fixed effect, δ_t is a separate fixed effect for every calendar year-month, and $\mathbf{x}_{it}$ contains the $K = 12$ controls in Table 2. National monthly shocks and common seasonality are absorbed by δ_t, while observed local weather varies across districts within a month. Standard errors for this benchmark are clustered by district. Heterogeneous staggered adoption and interference preclude interpreting its coefficient automatically as an average causal effect.

To describe spatially connected outcomes and regressors, we estimate

$$\begin{aligned}\mathbf{Y}_t = \rho W\mathbf{Y}_t + \beta\mathbf{LEZ}_t + \theta W\mathbf{LEZ}_t + \mathbf{X}_t\gamma + W\mathbf{X}_t\eta \\ + \boldsymbol{\alpha} + \delta_t\mathbf{1}_N + \boldsymbol{\varepsilon}_t.\end{aligned} \tag{2}$$

$\mathbf{Y}_t$ and $\mathbf{LEZ}_t$ are $N \times 1$ vectors, W is $N \times N$, and $\mathbf{X}_t$ is $N \times K$ with row i equal to $\mathbf{x}_{it}'$. Thus $(\mathbf{X}_t\gamma)_i = \sum_{k=1}^{K} x_{ikt}\gamma_k$ and $(W\mathbf{X}_t\eta)_i = \sum_j w_{ij} \sum_k x_{jkt}\eta_k$. The scalar β belongs to own designation, θ to neighboring designation, and γ and η are distinct control-coefficient vectors. The spatial autoregressive parameter ρ links contemporaneous outcomes; it is not a temporal lag.

The baseline W gives equal weights to the five nearest district polygon centroids, using the largest polygon component for multipart districts and projected coordinates (EPSG:5179). Its diagonal is zero and each row sums to one. This construction assigns neighbors to every retained district despite uneven geographic density, with distances varying across districts. It need not form a single connected graph. Five neighbors provides a transparent geographic baseline, with three and seven neighbors assessed on the same sample. The directed matrix is fixed over time and represents geographic proximity rather than a measured atmospheric-transport radius or observed wind, commuting, or freight flows (Elhorst, 2014; LeSage & Pace, 2009).

If $A = I_N - \rho W$ is invertible, rearranging Equation (2) gives

$$\mathbf{Y}_t = A^{-1}\big[(\beta I_N + \theta W)\mathbf{LEZ}_t + \mathbf{X}_t\gamma + W\mathbf{X}_t\eta + \boldsymbol{\alpha} + \delta_t\mathbf{1}_N + \boldsymbol{\varepsilon}_t\big]. \tag{3}$$

Holding controls and fixed effects constant, the model-implied designation-response matrix is therefore

$$S_{\mathrm{LEZ}}(W) = A^{-1}(\beta I_N + \theta W), \qquad [S_{\mathrm{LEZ}}(W)]_{ij} = \frac{\partial \widehat{Y}_{it}}{\partial \mathrm{LEZ}_{jt}}. \tag{4}$$

Column j describes the fitted concentration changes across districts when district j's designation changes, including spatial feedback. Because the model is linear, its

column also gives the fitted 0-to-1 contrast for a binary designation change. Following spatial impact decomposition (Elhorst, 2010; LeSage & Pace, 2009), the average direct association is $N^{-1}\,\mathrm{tr}(S_{\mathrm{LEZ}})$, the total is $N^{-1}\mathbf{1}_N' S_{\mathrm{LEZ}}\mathbf{1}_N$, and the indirect association is their difference. The total simplifies to $(\beta+\theta)/(1-\rho)$ for row-standardized W. The same matrix applies to every month within a fitted specification; seasonal models estimate separate matrices. These equally district-weighted quantities are neither a staggered-adoption average treatment effect nor a population-weighted exposure or health effect.

Dependence-aware inference and seasonal comparisons

Point estimates use the two-way within `spml()` specification in `splm`, with a spatial outcome lag and no spatial-error term (Millo & Piras, 2012). A Gaussian likelihood supplies the working criterion; score-based covariance estimation allows dependence as described below. Structural interpretation requires a correctly specified mean, valid regressor-exogeneity conditions, and an appropriate spatial process.

We calculate the joint observed information for ρ, the regression coefficients, and log error variance, retaining their cross-covariances. Monthly scores aggregate across all districts. A score-based heteroskedasticity and autocorrelation consistent (HAC) sandwich uses a Bartlett kernel and a maximum lag of 12 calendar months; bandwidths of 6 and 24 months assess sensitivity. This follows the cross-sectional aggregation approach to dependent-panel inference (Belotti, Hughes, & Piano Mortari, 2017; Driscoll & Kraay, 1998). The delta method propagates joint uncertainty to the spatial associations, with approximate 95% confidence intervals based on 1.96 standard errors. The procedure permits contemporaneous cross-sectional dependence and weak temporal dependence in the scores, but not arbitrary mean misspecification. The covariance estimator is detailed in Supplementary Section S5.

Seasonal models re-estimate Equation (2) using December–February (winter), March–May (spring), June–August (summer), or September–November (autumn). Each retains 39 original calendar months and 9,633 district-months, with its own coefficients and fixed effects. December and the following January–February are not aggregated into a winter-year outcome. A supplementary May–June ozone model uses 26 months, motivated by prior atmospheric evidence (Oak et al., 2025).

We formally compare the four seasonal totals using a three-degree-of-freedom Wald test. Seasonal score influences are aligned on the complete 156-month calendar to retain cross-season serial covariance; months absent from a seasonal fit contribute zero. Holm adjustment (Holm, 1979) is applied across ten omnibus tests (five pollutants,

baseline and cohort-trend models), and separately across all 60 pairwise seasonal comparisons. Five pooled baseline total-association tests form a separate Holm-adjusted family. These are exploratory, not preregistered confirmatory tests. Displayed intervals remain marginal and are not simultaneous or multiplicity-adjusted. Inference is approximate, especially with only 39 observed months per seasonal model; full covariance construction appears in Supplementary Section S6.

Sensitivity analyses

To assess differential regional trajectories, we add separate linear calendar-time trends for the three adoption cohorts and their spatial lags, both in pooled and seasonal models. Baseline and trend-adjusted specifications offer complementary comparisons: the added trends can absorb gradual policy-related change as well as pre-existing trajectories. We also omit each treated cohort in turn, remove its districts in every month, and rebuild the neighbor matrix. This assesses how cohort composition and its associated spatial links influence the findings.

Other models vary neighbor count, omit transport or land-use controls, or start in 2013 with the same covariates. Timing scenarios change one cohort's assigned month while retaining the sample, controls, neighbor matrix, and geographic cohort-trend membership; they are coding alternatives, not probabilistic bounds on implementation error. Baseline and cohort-trend SDMs are also fitted to the nearest-station panel. All specified results are reported without significance screening.

Results and discussion

Pre-adoption trajectories

Pre-adoption diagnostics characterize the regional trajectories relevant to interpreting later contrasts. The joint Wald tests reject zero pre-adoption contrasts for all five pollutants under both outcome-regression and doubly robust adjustment, in both observation periods. Primary-panel maximum-$|t|$ p-values are below 0.001 for all regression-adjusted outcomes. Under doubly robust adjustment, SO_2 has $p = 0.0065$ and the other four have $p < 0.001$ (Supplementary Table S1).

Figure 2 displays the timing of these differences, with unbinned monthly contrasts and simultaneous bands. The adjusted trajectories differ between designated and comparison districts before adoption, supporting an associational interpretation of the post-adoption profile. Cohort support also changes at the endpoint: the 2020 cohort

is observed through event month 59 and does not contribute at month 60. The consistency of the pre-adoption findings across adjustment methods makes regional-trend sensitivity a central part of the subsequent spatial analysis (Supplementary Figure S1).

Pooled monthly associations

To distinguish a non-spatial summary from associations incorporating cross-district feedback, we estimate Equations (1) and (2) on the same sample. Table 3 presents the benchmark coefficient and the SDM decomposition. All fits contain 247 districts, 156 months, the listed controls, and district and calendar year-month fixed effects.

The baseline NO_2 total is -1.868 ppb (HAC standard error 0.519; 95% confidence interval $[-2.886, -0.850]$), equivalent to -6.3% of the designated districts' pre-adoption mean. It remains distinguishable from zero across the five pooled outcome tests after Holm adjustment ($p = 0.0016$). Its direct component is small (0.102 ppb); the negative total is primarily allocated to the indirect component (-1.970 ppb). The decomposition locates the fitted association mainly across units, adding regional information beyond the own-designation coefficient. Its atmospheric interpretation is considered below.

The O_3 total is 0.563 ppb (95% confidence interval $[-0.156, 1.283]$); the CO total is -7.128 ppb ($[-19.506, 5.250]$). SO_2 and PM_{10} total intervals likewise include zero. For CO and PM_{10}, direct and indirect components differ in sign. Full coefficients appear in Supplementary Table S4.

Residual dependence materially affects precision. Median district-level lag-1 correlations range from 0.705 to 0.776, lag-12 correlations from 0.341 to 0.469, and monthly residual Moran's I medians from -0.016 to 0.033 (Supplementary Table S5). Relative to joint-information standard errors, HAC(12) increases the NO_2 total standard error from 0.168 to 0.519 and the O_3 standard error from 0.192 to 0.367. The ozone interval includes zero under all three HAC bandwidths, while the NO_2 interval remains negative (Supplementary Table S6).

Seasonal contrasts and trend sensitivity

Separate seasonal fits identify within-year patterns alongside the pooled summaries. Figure 3 shows both baseline and cohort-trend-adjusted totals, and Supplementary Table S2 supplies all components. Baseline NO_2 totals are negative in winter (-1.183 ppb), spring (-1.976), summer (-2.176), and autumn (-1.849). The winter interval

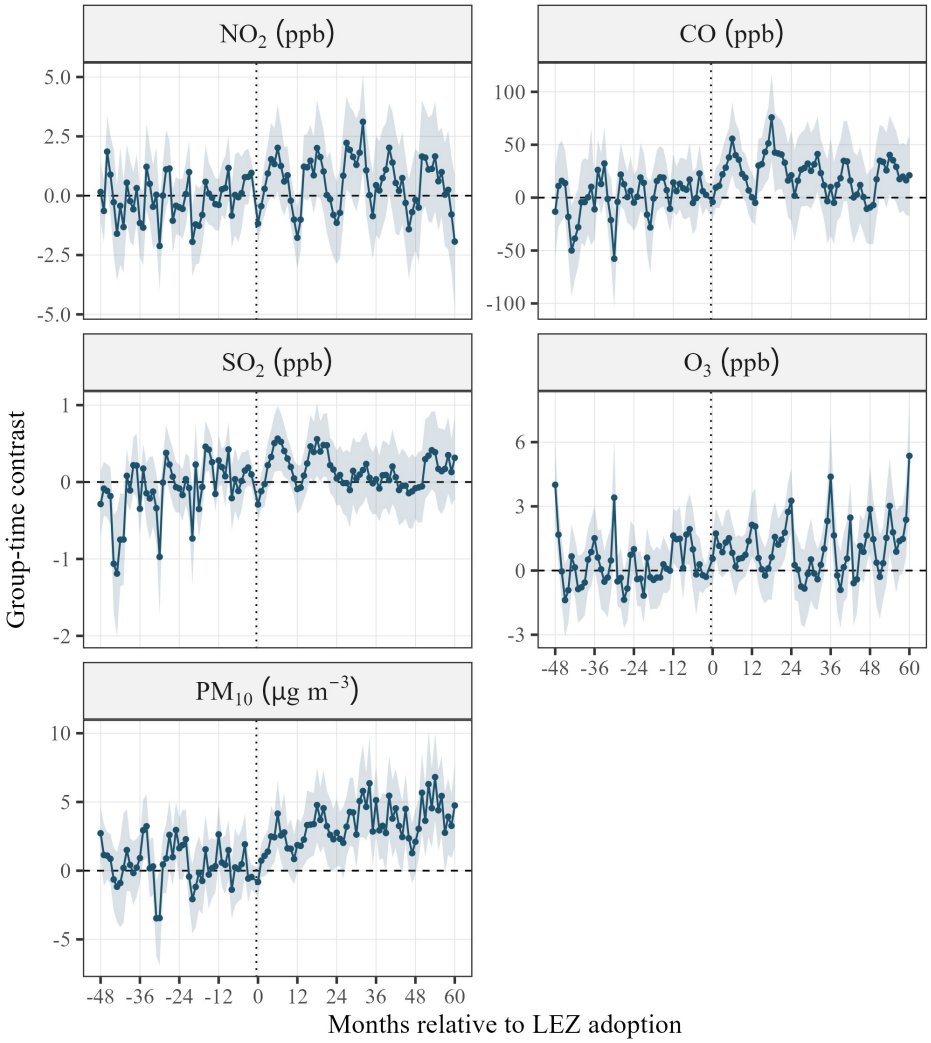


Fig. 2 Monthly event-study diagnostics, 2012–2024. Regression-adjusted group-time contrasts are aggregated by event month relative to assigned designation. Shading shows simultaneous 95% bands over months −48 to 60; month −1 is the universal reference. The vertical line separates pre- and post-designation observations. Bands use district multipliers without cross-district dependence adjustment.

Table 3 Pooled monthly associations: non-spatial benchmark and spatial decomposition

Outcome	TWFE	Direct	Indirect	Total	Total/mean (%)
NO_2	-1.874***	0.102	-1.970***	-1.868***	-6.3
	(0.210)	(0.099)	(0.533)	(0.519)	
CO	-10.542***	5.547**	-12.675**	-7.128	-1.3
	(3.380)	(2.582)	(6.216)	(6.315)	
SO_2	-0.273***	-0.042*	-0.042	-0.084	-1.6
	(0.060)	(0.024)	(0.070)	(0.082)	
O_3	1.102***	-0.041	0.604*	0.563	2.4
	(0.137)	(0.102)	(0.353)	(0.367)	
PM_{10}	0.905***	-0.770***	0.662	-0.108	-0.2
	(0.252)	(0.272)	(0.831)	(0.778)	

Standard errors in parentheses.

TWFE: unit-clustered SEs; spatial effects: HAC(12) SEs.

$^{*}p < 0.10$, $^{**}p < 0.05$, $^{***}p < 0.01$.

Notes: TWFE: Equation (1); direct, indirect, and total: Equations (2)–(4). Parentheses contain district-clustered (TWFE) or score-HAC(12) delta-method (SDM) standard errors. Units follow Table 1. The final column scales totals by pre-LEZ means, not counterfactual outcomes.

includes zero, and the formal equality test does not distinguish the four totals (unadjusted $p = 0.342$). Thus, the common negative baseline direction is accompanied by insufficient evidence of a seasonal difference.

Baseline ozone totals are -0.650 ppb in winter, 1.366 in spring, 1.882 in summer, and -0.009 in autumn. The seasonal-equality test rejects after adjustment across ten omnibus comparisons (Holm-adjusted $p < 0.001$). Spring minus winter is 2.016 ppb (standard error 0.427) and summer minus winter is 2.532 ppb (0.557); both adjusted pairwise p-values are below 0.001 across all 60 comparisons. This identifies a baseline seasonal contrast that the pooled ozone total obscures. The additional May–June ozone total is 2.680 ppb (standard error 0.741), providing a complementary description of an overlapping window rather than an independent replication.

SO_2 also shows baseline seasonal heterogeneity (Holm-adjusted $p < 0.001$): its winter total is -0.468 ppb (95% interval $[-0.611, -0.324]$), whereas the other three seasonal intervals include zero. CO and PM_{10} show neither a rejected baseline seasonal-equality test nor individual baseline seasonal totals distinguishable from zero. After cohort-trend adjustment, no pollutant's seasonal-equality test rejects; ozone has unadjusted $p = 0.180$ and SO_2 has $p = 0.370$, both with Holm-adjusted $p = 1.000$. Supplementary Table S7 reports all omnibus tests.

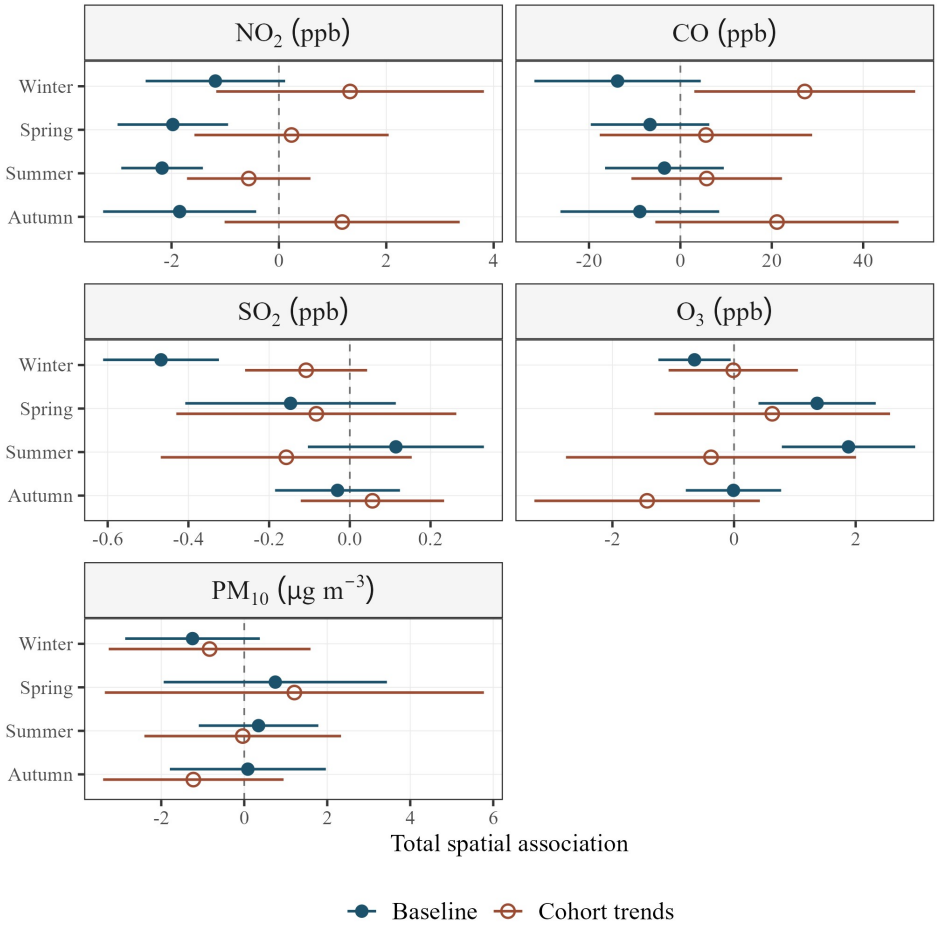


Fig. 3 Seasonal total spatial associations with and without cohort-specific trends. Filled and open points distinguish the baseline and trend-adjusted specifications; horizontal bars are marginal 95% score-HAC(12) delta-method intervals. Each fit uses 247 districts and 39 months, with separate district and year-month fixed effects. Axes differ between pollutants. Formal cross-season tests retain cross-season covariance and are reported in Supplementary Table S7; overlapping or non-overlapping marginal intervals are not themselves those tests.

Pooled model sensitivity

To assess whether the pooled results depend on a particular rollout cohort or on differential trajectories, Table 4 compares cohort omissions and the trend specification. The NO_2 total remains negative after each cohort omission, ranging from -2.610 to -1.312 ppb. Other pollutants depend more strongly on cohort composition: excluding Seoul changes the CO total to 2.165 ppb and the O_3 total to 0.156 ppb. These comparisons assess the joint influence of the omitted cohort and its associated spatial links.

Adding cohort trends changes the NO_2 total to 0.530 ppb (standard error 0.864), CO to 14.481 ppb (7.289), and O_3 to -0.254 ppb (0.858). Four total intervals include zero. CO's marginal interval is just above zero ($[0.194, 28.767]$; unadjusted $p = 0.047$), but this exploratory result is outside the five-test baseline multiplicity adjustment. Its changed sign indicates sensitivity to regional-trend specification.

Table 4 Sensitivity of pooled total spatial associations to trends and cohort composition

Specification	NO_2	CO	SO_2	O_3	PM_{10}
Monthly baseline	-1.868***	-7.128	-0.084	0.563	-0.108
	(0.519)	(6.315)	(0.082)	(0.367)	(0.778)
Cohort trends	0.530	14.481**	0.001	-0.254	0.159
	(0.864)	(7.289)	(0.086)	(0.858)	(0.847)
Omit Seoul cohort	-1.312***	2.165	-0.014	0.156	0.357
	(0.482)	(6.993)	(0.094)	(0.519)	(0.852)
Omit July 2018 cohort	-2.610***	-15.854**	0.011	0.978***	0.465
	(0.611)	(7.217)	(0.107)	(0.366)	(0.851)
Omit January 2020 cohort	-2.016***	-12.473	-0.054	0.544	0.597
	(0.651)	(8.147)	(0.077)	(0.344)	(0.989)

HAC(12) standard errors in parentheses.

$^{*}p < 0.10$, $^{**}p < 0.05$, $^{***}p < 0.01$.

Notes: Parentheses contain score-HAC(12) standard errors. Trends and their spatial lags are added for each adoption cohort. Cohort omissions retain 222, 212, and 234 districts and rebuild W. Units follow Table 1.

The remaining geographic, control, and period checks appear in Supplementary Table S3. NO_2 totals retain a negative direction with three or seven neighbors, a 2013 start, and omission of land-use controls, although magnitudes vary. Other pollutants are more sensitive to geographic weights and transport adjustment. Across the timing scenarios, baseline NO_2 totals range from -1.852 to -1.840 ppb, with intervals below

zero; trend-adjusted totals range from 0.606 to 0.654 ppb, with intervals including zero (Supplementary Table S11). The NO_2 association is therefore more sensitive to the trend specification than to these assigned-month alternatives. CO's marginal trend-adjusted interval includes zero under the January 2018 and December 2020 alternatives.

Prediction validation and interpolation sensitivity

To assess the measurement layer independently of policy-model significance, we compare held-out station predictions and then re-estimate the pooled models on a common-support nearest-station panel. IDW has lower leave-one-station-out RMSE than nearest prediction for all 16 constructed environmental series. For the urban ambient outcomes, RMSEs are 4.630 ppb for NO_2, 98.241 ppb for CO, 1.191 ppb for SO_2, 4.155 ppb for O_3, and 5.793 $\mu g/m^3$ for PM_{10} (Supplementary Table S8). The low-wind equivalent has an RMSE of 7.595 days, indicating considerable prediction uncertainty despite complete district-month coverage.

For precipitation, IDW RMSE rises from 1.422 mm/day under station holdout to 1.700 under 100-km grid-block exclusion; the corresponding nearest values are 1.636 and 1.769. The blocked comparison does not favor IDW on every metric: its mean absolute error is 0.989, versus 0.983 for nearest prediction. These are pooled point-prediction diagnostics, not independent monthly replicates or validation of unknown district means.

Under common-support nearest interpolation, the baseline NO_2 total is -1.831 ppb (95% interval $[-2.825, -0.837]$), close to the IDW result. SO_2 and PM_{10} totals change to -0.487 ppb and -2.377 $\mu g/m^3$, with marginal intervals below zero, unlike their IDW counterparts. With nearest interpolation plus cohort trends, all five pooled intervals include zero (Supplementary Table S9). Thus, NO_2 is similar across interpolations but trend-sensitive, whereas SO_2 and PM_{10} also depend on concentration-field construction.

Atmospheric interpretation

The strongest pooled baseline signal is a negative NO_2 total, largely allocated to the SDM's cross-unit component. This pattern is consistent with the traffic-related relevance of NO_2 and motivates assessment beyond individual district boundaries. Its mechanistic interpretation nevertheless encompasses emissions and atmospheric conversion, concurrent metropolitan policies, and the regional trajectories captured by cohort trends. The spatial decomposition is a fitted association rather than a direct

measurement of atmospheric transport or diesel-emission reductions. For CO, SO_2, and PM_{10}, the intervals allow a range of associations, reflecting differences in source mixtures, atmospheric lifetimes, background contributions, and estimation precision (Holman et al., 2015; Seinfeld & Pandis, 2016).

Ozone illustrates the information gained by seasonal analysis alongside a pooled concentration summary. The baseline formal tests identify a spring–summer versus winter contrast, which is compatible with seasonally varying chemistry and transport. Reduced removal of ozone by reaction with NO (NO titration) is distinct from a change in net photochemical ozone production under volatile-organic-compound (VOC)-limited conditions. Either can contribute to an ozone increase after precursor changes; distinguishing their contributions requires chemical observations beyond a monthly regression coefficient. Korean observational evidence documents changing chemical regimes (Oak et al., 2025), and multi-model emission-reduction experiments show that ozone response direction and magnitude depend on chemical regime and concentration metric (Bessagnet et al., 2024). The observed, trend-sensitive seasonal contrasts provide empirically grounded hypotheses for atmospheric investigation. NO and VOC observations, chemical-regime indicators, and transport-aware analysis would enable direct evaluation of the candidate mechanisms.

For SO_2, the negative winter baseline association is compatible with seasonally varying source mixtures and dispersion; its change after cohort-trend adjustment emphasizes the role of regional trajectories in this interpretation. For particulate matter, a coarse mass metric combines road and non-road sources and secondary particles. The PM_{10} interval spanning zero leaves open changes in finer particles or composition, which require additional measurements. The interpolation sensitivity of SO_2 and PM_{10} further identifies concentration-field construction as a relevant dimension of their assessment. Comparisons with studies of broader Korean air-quality packages place these patterns in context, while recognizing differences in geographic coverage, policy bundles, periods, and identification strategies (Im et al., 2026; Park & Lim, 2025).

Implications for environmental monitoring and assessment

The assessment directs monitoring priorities toward the sources of uncertainty relevant to each pollutant. Prediction accuracy informs concentration-field construction, while interpolation and trend comparisons identify which analytical choices shape the fitted associations. Station coverage, changing network composition, and distance to contributing observations are priorities for regional estimates. Historical station records

would help quantify whether changes in an interpolated series reflect environmental change or changes in the contributing sites.

Two design principles follow. First, retain seasonal resolution to capture within-year patterns obscured by pooled summaries. Second, compare interpolation methods using the same geographic target, eligible observations, and aggregation weights, with prediction performance assessed independently of policy-model significance. Road-flow and wind-directed exposure mappings could complement the geographic-neighbor model with mechanism-specific connections validated against independent information.

The reported quantities describe district-level ambient conditions: equal district weighting gives a small county and a densely populated urban district the same weight, and monthly mean ozone differs from daily maximum eight-hour exposure. Assessment of individual exposure, health benefits, or regulatory compliance would require corresponding temporal metrics and spatial weights. Within its current scope, the analysis supports monitoring priorities and evaluation design rather than causal effectiveness rankings of districts or seasons.

Scope, limitations, and future directions

Differential regional trajectories remain the principal constraint on causal attribution. Fixed effects absorb time-invariant district differences and common monthly shocks, but not necessarily metropolitan-specific policies, fleet turnover, or heterogeneous responses to national events. Spatial outcome lags address dependence, not pre-adoption comparability, and cohort trends are a sensitivity assessment rather than a verified counterfactual. The findings therefore remain conditional associations.

District-specific enforcement histories are needed to resolve within-year timing and implementation differences, particularly for the assumed third-phase month. Earlier Seoul restrictions and the 2016 announcement also raise questions of prior exposure and anticipation. Stronger causal and mechanism-based evaluation would combine credible comparison trajectories with enforcement, vehicle-eligibility, compliance, and fleet-composition data, distinguishing mediators from confounding factors.

Measurement priorities include complete historical pollution-station matching and fixed-boundary correspondence. Kriging and exact Thiessen–district aggregation would extend the common-grid comparison (Esri, n.d.; Pebesma, n.d.), and spatially blocked validation could be extended from precipitation to pollutants. Interpolation may contribute to covariance in outcomes and controls; station holdouts do not establish district-mean accuracy. Score-HAC intervals neither propagate this measurement

uncertainty nor correct mean misspecification. Annual controls retain district-year resolution. Seasonal inference remains approximate with 39 observed months, and the 2020 cohort contains only 13 districts.

Conclusions

This study integrates monitoring-data validation, spatial decomposition, and seasonal comparisons in a reproducible assessment of metropolitan vehicle restrictions. The negative baseline NO_2 association is similar across two interpolations but sensitive to cohort trends; ozone and SO_2 seasonal contrasts also depend on trend assumptions, while SO_2 and PM_{10} pooled estimates vary with field construction. Pre-adoption differences support an associational rather than causal interpretation. By separating measurement sensitivity from regional-trend sensitivity, the workflow provides a transparent basis for targeted validation, monitoring priorities, and subsequent LEZ evaluation.

Statements and Declarations

Funding. No external funding was received for this study.

Competing interests. The authors have no relevant financial or non-financial competing interests to disclose.

Author contributions. Minju Lee: Conceptualization, Methodology, Formal analysis, Data curation, Visualization, Writing - original draft. Mijeong Kim: Conceptualization, Methodology, Supervision, Writing - review & editing, Project administration.

Data availability. Original monitoring observations and station information are available from the AirKorea and KMA sources cited in Materials and methods; annual transport and land-use statistics are available through KOSIS. The analysis datasets derived from these sources are not publicly available because of copyright and redistribution restrictions.

Code availability. The code used for the analyses in this paper, together with the corresponding output results, is available at https://github.com/MJLee25/korea-lez-air-quality.

Ethics approval and consent. Not applicable. The study analyzes environmental monitoring and aggregate district statistics and does not involve human participants, individual participant records, or animal experiments.

Ethical responsibilities of authors. Both authors have reviewed the applicable ethical responsibilities and confirm compliance with the journal's requirements.

Use of AI-assisted technologies. OpenAI Codex assistance is disclosed in Materials and methods. The authors retain responsibility for the submitted work.

References

AirKorea (n.d.). *Final-confirmed hourly air-quality observations: data downloads.* https://www.airkorea.or.kr/web/last_amb_hour_data?pMENU_NO=123 (Accessed 14 September 2026)

Belotti, F., Hughes, G., Piano Mortari, A. (2017). Spatial panel-data models using Stata. *The Stata Journal*, *17*(1), 139–180, https://doi.org/10.1177/1536867X1701700109

Bessagnet, B., Cuvelier, K., de Meij, A., Monteiro, A., Pisoni, E., Thunis, P., ... Trimpeneers, E. (2024). Assessment of the sensitivity of model responses to urban emission changes in support of emission reduction strategies. *Air Quality, Atmosphere & Health*, *17*, 681–706, https://doi.org/10.1007/s11869-023-01469-z

Callaway, B., & Sant'Anna, P.H.C. (2021). Difference-in-differences with multiple time periods. *Journal of Econometrics*, *225*(2), 200–230, https://doi.org/10.1016/j.jeconom.2020.12.001

Delgado, M.S., & Florax, R.J.G.M. (2015). Difference-in-differences techniques for spatial data: Local autocorrelation and spatial interaction. *Economics Letters*, *137*, 123–126, https://doi.org/10.1016/j.econlet.2015.10.035

Driscoll, J.C., & Kraay, A.C. (1998). Consistent covariance matrix estimation with spatially dependent panel data. *The Review of Economics and Statistics*, *80*(4), 549–560, https://doi.org/10.1162/003465398557825

Elhorst, J.P. (2010). Applied spatial econometrics: Raising the bar. *Spatial Economic Analysis*, *5*(1), 9–28, https://doi.org/10.1080/17421770903541772

Elhorst, J.P. (2014). *Spatial econometrics: From cross-sectional data to spatial panels.* Heidelberg: Springer. (https://doi.org/10.1007/978-3-642-40340-8)

Esri (n.d.). *Create Thiessen polygons (analysis).* https://pro.arcgis.com/en/pro-app/3.3/tool-reference/analysis/create-thiessen-polygons.htm (ArcGIS Pro 3.3 documentation. Accessed 11 September 2026)

Holm, S. (1979). A simple sequentially rejective multiple test procedure. *Scandinavian Journal of Statistics*, *6*(2), 65–70, https://www.jstor.org/stable/4615733

Holman, C., Harrison, R., Querol, X. (2015). Review of the efficacy of low emission zones to improve urban air quality in european cities. *Atmospheric Environment*, *111*, 161–169, https://doi.org/10.1016/j.atmosenv.2015.04.009

Im, J., Jang, Y., Kim, S., Hong, J.H. (2026). Pollutant-specific effects of urban air policy: Causal evidence from South Korea's Clean Air Act. *Urban Climate*, *65*, 102809, https://doi.org/10.1016/j.uclim.2026.102809

Korea Environment Corporation (n.d.). *AirKorea monitoring-station information: Open API.* https://www.data.go.kr/data/15073877/openapi.do (Korea Public Data Portal. Accessed 14 September 2026)

Korea Land and Geospatial Informatix Corporation (n.d.). *Urban area per capita by province, city, county, and district.* https://kosis.kr/statHtml/statHtml.do?orgId=101&tblId=DT_1YL20421E&conn_path=I3 (Accessed 17 August 2026)

Korea Meteorological Administration (n.d.-a). *Daily surface observations from the Automated Synoptic Observing System (ASOS): Open API.* https://www.data.go.kr/data/15059093/openapi.do (Korea Public Data Portal. Accessed 14 September 2026)

Korea Meteorological Administration (n.d.-b). *Past weather observations by element: Station-year precipitation tables.* https://www.weather.go.kr/w/weather/land/past-obs/obs-by-element.do?stn=108&yy=2012&obs=21 (Accessed 28 September 2026)

Korea Transportation Safety Authority (n.d.). *Vehicle kilometers traveled statistics: Vehicle kilometers traveled by vehicle use, vehicle type, and fuel type.* https://kosis.kr/statHtml/statHtml.do?orgId=426&tblId=DT_426001_N004&conn_path=I3 (Accessed 17 August 2026)

LeSage, J.P., & Pace, R.K. (2009). *Introduction to spatial econometrics.* Boca Raton, FL: CRC Press. (https://doi.org/10.1201/9781420064254)

MECAR (n.d.). *Information portal for old diesel vehicle operating restriction.* https://www.mecar.or.kr/dr/info/oldDieselCarAlwaysDr.do (Accessed 7 September 2026)

Millo, G., & Piras, G. (2012). splm: Spatial panel data models in R. *Journal of Statistical Software*, *47*(1), 1–38, https://doi.org/10.18637/jss.v047.i01

Ministry of Culture, Sports and Tourism (2017). *Policy briefing: Changes in the new year—environment, public safety, administration, and defence.* Weekly Gonggam, No. 387, 9 January, p. 36. https://www.korea.kr/goNewsRes/attaches/2019.05/23/107_20170109_01IozeNoYDGJM000.pdf (In Korean. Accessed 30 September 2026)

Ministry of Environment (2016). *Restrictions on old diesel vehicles in Seoul from the following year.* Korea Policy Briefing, 4 August 2016. https://www.korea.kr/news/policyNewsView.do?newsId=148819495 (In Korean; accessed 7 September 2026)

Ministry of Land, Infrastructure and Transport (n.d.). *Motor vehicle registrations per capita by province, city, county, and district.* https://kosis.kr/statHtml/statHtml.do?orgId=101&tblId=DT_1YL20731&conn_path=I3 (Accessed 17 August 2026)

Nieuwenhuijsen, M.J. (2016). Urban and transport planning, environmental exposures and health-new concepts, methods and tools to improve health in cities. *Environmental Health*, *15*(Suppl 1), S38, https://doi.org/10.1186/s12940-016-0108-1

Oak, Y.J., Jacob, D.J., Pendergrass, D.C., Dang, R., Colombi, N.K., Chong, H., ... Kim, J. (2025). Air quality trends and regimes in South Korea inferred from 2015–2023 surface and satellite observations. *Atmospheric Chemistry and Physics*, *25*, 3233–3252, https://doi.org/10.5194/acp-25-3233-2025

Park, D., & Lim, B.I. (2025). The effect of the ultra-low emission zone on $PM_{2.5}$ concentration in Seoul, South Korea. *Atmospheric Environment*, *340*, 120908, https://doi.org/10.1016/j.atmosenv.2024.120908

Pebesma, E. (n.d.). *Simple, ordinary or universal, global or local, point or block kriging, or simulation.* https://r-spatial.github.io/gstat/reference/krige.html (gstat reference documentation. Accessed 11 September 2026)

612 Seinfeld, J.H., & Pandis, S.N. (2016). *Atmospheric chemistry and physics: From air*
613 *pollution to climate change* (3rd ed.). John Wiley & Sons.

Supplementary Files

This is a list of supplementary files associated with this preprint. Click to download.

- TableS2.tex
- TableS7.tex
- TableS9.tex
- TableS4.tex
- TableS1.tex
- TableS3.tex
- TableS5.tex
- TableS11.tex
- TableS8.tex
- TableS6.tex
- FigS1.jpg
- OnlineResource1.tex
- OnlineResource1.pdf